Journal of the Korean Society
for Marine Environmental Engineering
Vol. 3, No. 4. pp. 37~55, November 2000

Characteristics of Flow and Sedimentation around the Embankment

by
Moon Ock Lee[1], Il Heum Park[1] and Yeon Gyu Lee[2]

방조제 부근에서의 흐름과 퇴적환경의 특성

이문옥[1], 박일흠[1], 이연규[2]

Abstract

Two-dimensional numerical experiments and field surveys have been conducted to clarify some environmental variations in the flow and sedimentation in the adjacent seas after the construction of a tidal embankment. Velocities of flow and water levels in the bay decreased after the construction of the barrage. When the freshwater was instantly released into the bay, the conditions of flow were unaltered, with the exception of a minor variation in velocities and tidal levels around the sluices at the ebb flow. The computational results showed that freshwater released at the low water reached the outside of the bay and then returned to the inside with the tidal currents at the high water. The front sea regions of the embankment had a variety of sedimentary phases such as a clayish silt, a silty clay and a sandy clayish silt. However, a clayish silt was prevalent in the middle of the bay. On the other hand, the skewness, which reflects the behaviour of sediments, was ± 0.1 at the front regions of the embankment while it was more than ± 0.3 in the middle of the bay. Analytical results of drilling samples acquired from the front of the sluice gates showed that the lower part of the sediments consists of very fine silty or clayish grains. The upper surface layer consisted of shellfish, such as oyster or barnacle with a thickness of 40~50 cm. Therefore, it seemed that the lower part of the sediments would have been one of intertidal zones prior to the embankment construction while the upper shellfish layer would have been debris of shellfish farms formed in the adjacent seas after the construction of the embankment. This shows the difference of sedimentary phases reflected the influence of a tidal embankment construction.

요 약

전라남도 고흥반도에 인접한 해창만의 어장환경문제와 관련하여 방조제 축조후 주변해역에서의 흐름과 퇴적환경의 변화를 파악하고 특히 수문개방시 일시에 다량으로 방류되는 담수가 인근해역에 미치는 영향을 파악하기 위하여 1997년과 1998년의 두 차례에 걸친 현장조사

(1) Member,, Yosu National University, moleel@cholian.net
(2) Yosu National University

와 해수유동 및 담수확산에 관한 2차원 수치실험을 실시하였다. 방조제 체절후에는 체절전에 비하여 유속이 전반적으로 크게 감소하였고 조위는 방조제 부근에서 그 진폭이 다소 감소하였다. 방조제 수문을 통하여 담수를 방류한 경우, 전반적인 흐름 형태는 무방류시에 비하여 큰 차이가 없었으나, 간조시의 경우 방류한 담수의 영향으로 수문 부근에서 유속과 조위가 각각 다소의 변화를 나타내었다. 담수확산의 수치실험결과, 간조시에 담수는 만외까지 유출하지만, 만조시에는 서류하는 조류를 타고 다시 만의 안쪽까지 되돌아오는 경향을 보였다. 방조제 전면해역에서는 점토질의 실트, 실트질의 점토 및 사질점토질의 실트 등 다양한 퇴적상을 보였으나, 만의 중앙부에서는 점토질의 실트가 지배적이었다. 또한 퇴적물의 유동을 반영하는 왜도분포에서는 방조제 전면 해역에서 ±0.1, 만의 중앙부에서 +0.3 이상으로 양자간에 현저한 차이를 보였다. 방조제 전면해역에서 시추한 시료의 분석결과, 하부는 실트와 점토질의 세립의 퇴적상으로 구성되어 있지만, 상부의 표층은 두께 약 40~50 cm정도의 굴, 바지락 등으로 구성된 패각층이 분포하였다. 이와 같은 하부의 퇴적상은 방조제 축조전의 조간대 퇴적상으로 추정되며, 상부의 패각층은 제방 축조후 주변해역에 형성된 패류 양식장으로부터 기인한 잔해일 가능성이 컸다. 즉, 이와 같은 퇴적상의 차이는 방조제 축조의 영향을 반영하고 있는 것으로 판단되었다.

Keywords : idal embankment(방조제), sluice gates(수문), freshwater dispersion(담수확산),sedimentary environment(퇴적환경), drilling sampling(시추시료채취), numerical experiment(수치실험)

1. INTRODUCTION

Haechang Bay is located between the Kohung Peninsula and the Narodo Islands at the south of Korea(see Fig. 1) and is a relatively shallow sea receiving the effluents of the natural river so that aquaculture of shellfish and algae have been activated for a long time. However, in 1963 a tidal embankment was completed with electrical sluice gates to create agricultural lands at the downstream after some reclamation work. Although the seawater intrusion and water level towards upstream have been controlled, the biomass production at the sea side of the embankment has been severely affected because large amounts of freshwater are instantly released, especially at the ebb flow, through the sluice gates and into the adjacent fishing grounds.

This paper describes environmental changes regarding the flow and sedimentation in adjacent seas after the construction of a tidal embankment. Furthermore, and the most important thing for this study is to make sure of the behaviour of freshwater effluents, which are released from the sluice gates, through a field observation and numerical experiments.

2. MATERIAL AND METHODS

2.1. Field Observation

Field observations have been carried out to collect the data of tidal levels and currents at some given points in Haechang Bay twice during July 21~22, 1997(the age of moon : 16.3~17.3) and April 11~22, 1998(the age of moon : 14.0~15.0), as shown in Fig. 1. Firstly, a sequence of tidal levels for 25 hours was recorded with a tidal gauge(model type : Aanderra WLR7) and then, using self-recording current meters(model type : Valeport 105 and Alec ACM-16M, ACM-200PC), successive simultaneous measurements of tidal currents at three different points were carried out for two tidal periods.

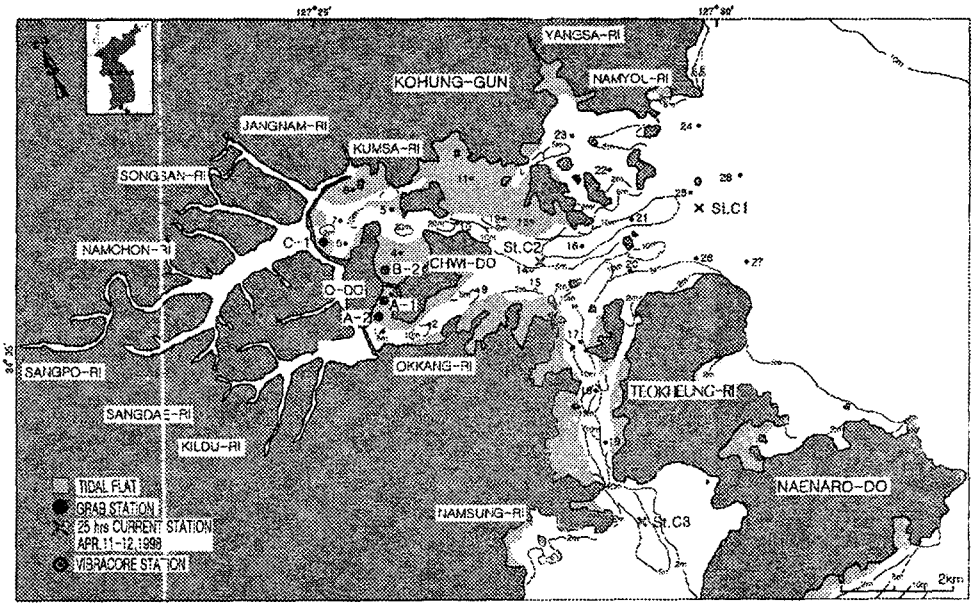

Fig. 1 Map showing the stations for water levels, currents and sediments sampling.

In order to work cut the influenced area due to released freshwater when the sluice gates were opened, the pursuit experiments of drogues and drift bottles were carried out twice at the ebb tides during July 21, 1997 and April 11, 1998. For the experiments, two small fishing boats and portable GPSs were used. A surface layer of sediment was sampled using a gravity core at 28 points and in addition to this, at 4 points ; of these the lower layer sediments were drilled by a vibra core and then grain sizes were analyzed, in order to investigate sedimentary phases near the embankment.

2.2. Numerical Experiments

Some numerical experiments have been completed not only to reproduce flow conditions before and after the construction of a tidal embankment, but also to investigate the phenomena of freshwater dispersion in the opening of the sluice gates. For the computations, the effect of stratification was not considered because the study area is shallow, less than 5 m in depth on the average, and therefore a two-dimensional numerical model with a depth integration was used. The numerical model uses moving boundaries in

Table 1. Categories and conditions of numerical experiments

run	conditions	categories	remarks
F-1	before closure of embankment		successive 8 tidal periods
F-2	after closure of embankment	no discharge	
F-3		discharged from the sluice gates 1, 2 and 3	

which the open boundary changes with depth variations. The open boundary conditions were controlled by water levels and velocities. The computational area has a system of 200×115 with a square grid size of 100 m for each case of before or after construction of a tidal embankment. The depth and bathymetrical data after construction of a tidal embankment was made based on the chart No. 240 published by the National Ocean Investigation Institute. The depth and bathymetrical data before the construction of the embankment was made based on not only the chart published by the Hydrographical Agency of Navy of Korea, but also the map published by the National Geographical Institute of Korea.

Table 1 represents the conditions and categories of numerical experiments for seawater movement. The computational results, run F-2 and run F-3, were used for outer forces in the numerical experiments of freshwater dispersion.

In particular, the freshwater dispersion area was obtained under the flow conditions of flood and the spring tide after two tidal periods from release to see the impact of a large quantity of freshwater released instantly on the fish farms.

(1) Fundamental equations of numerical model

The numerical model used for seawater movement is DIVAST(Depth Integrated Velocity and Solute Transport), originally developed by Falconer[1986]. Taking into account the resistances by wind and the sea bed into shear stress terms and after applying partial integrations of Leibniz vertically and continuity equations with a Boussinesq approximation, the depth integrated equations of momentum and continuity for seawater movement can be obtained as follows:

$$\frac{\partial UH}{\partial t} + \beta\left(\frac{\partial U^2 H}{\partial x} + \frac{\partial UVH}{\partial y}\right) - fVH + gH\frac{\partial \eta}{\partial x} - \frac{\rho_a C^* W_x \sqrt{W_x^2 + W_y^2}}{\rho} + \frac{gn^2 U\sqrt{U^2 + V^2}}{H^{1/3}} - \left[2\frac{\partial}{\partial x}\left(\varepsilon H\frac{\partial U}{\partial x}\right) + \frac{\partial}{\partial y}\left\{\varepsilon H\left(\frac{\partial U}{\partial y} + \frac{\partial V}{\partial x}\right)\right\}\right] = 0 \quad (1)$$

$$\frac{\partial VH}{\partial t} + \beta\left(\frac{\partial UVH}{\partial x} + \frac{\partial V^2 H}{\partial y}\right) + fUH + gH\frac{\partial \eta}{\partial y} - \frac{\rho_a C^* W_y \sqrt{W_x^2 + W_y^2}}{\rho} + \frac{gn^2 V\sqrt{U^2 + V^2}}{H^{1/3}} - \left[2\frac{\partial}{\partial y}\left(\varepsilon H\frac{\partial V}{\partial y}\right) + \frac{\partial}{\partial x}\left\{\varepsilon H\left(\frac{\partial U}{\partial y} + \frac{\partial V}{\partial x}\right)\right\}\right] = 0 \quad (2)$$

$$\frac{\partial \eta}{\partial t} + \frac{\partial UH}{\partial x} + \frac{\partial VH}{\partial y} = 0 \quad (3)$$

where, t is time, β is the correction coefficient of momentum, U, V are depth mean velocities in the x, y directions, respectively, H is a total depth, g is the gravitational acceleration, f is a Coriolis parameter, η is a displacement of sea surface, ε is depth mean eddy viscosity, ρ_a is a density of air, C^* is the resistance coefficient of sea surface, W_x , W_y are wind velocities in the x , y direction and n is the Manning's roughness.

All terms in the equations of (1), (2) and (3) are calculated in term of the ADI method with a centralized discretion in space, using a staggered grid scheme. Non-linear advective terms expressed by means of discreted equations are solved by iterative computations with a implicit method, The time step Δt can be taken up to 8 times larger than time step

given as the Courant number, in the equation (4).

$$\Delta t \leq 8\frac{\Delta x}{\sqrt{g h_{max}}} \quad (4)$$

where Δx is a grid size, h_{max} is a maximum depth in the domain.

The boundary of computational domain is divided into two parts, i.e., enclosed boundary on land and open boundary in rivers or in the sea. Any enclosed boundary with well developed wetlands is movable since the present numerical model takes a moving boundary system. Because in regions of tidal flood plains the numerical model must be capable of treating such flooding and drying phenomena by removing dry cells and replacing flood cells as the tidal ebbs and floods respectively. The boundaries of the modelling domain will therefore move throughout the tidal cycle. A widely used solution procedure for the treatment of flooding and drying has been developed by Leendertse *et al.*[1971]. However, this study has taken a new flooding and drying routine developed by Falconer *et al.*[1991]. Boundary conditions on the open boundary are composed to be controlled by water levels or velocities.

Water level variations on the open boundary in the model basin are given by a tidal motion. Tidal harmonic constituents used in the input of water levels are indicated in Table 2. The simulation of seawater behaviour has been examined using these amplitudes and lag phases shown in this table.

3. RESULTS AND CONSIDERATION

3.1 Current Circumstances

Fig. 2 shows stick diagrams of tidal currents simultaneously measured at the stations C1~C3 shown in Fig. 1. According to the results, the flood tidal current flow towards the northwest at stations C1 and C2 while they flow towards the south at station C3. The ebb tidal current flow towards the southeast at

Table 2 Tidal harmonic constituents used as open boundaries (National Ocean Investigation Institute, 1992)

station	M_2		S_2		K_1		O_1		position
	H (cm)	κ (°)	H (cm)	κ (°)	H (cm)	κ (°)	H (cm)	κ (°)	
Yosu	101	54	47	282	20	191	12	153	34°45′N, 127°46′E
Chobaldo	111	267	46	302	23	182	17	166	38′N, 33′E
Narodo	105	260	48	283	25	187	16	157	28′N, 27′E
Kumodo	98	255	48	286	20	179	15	152	35′N, 44′E
Keomundo	90	270	40	295	23	193	17	171	02′N, 19′E
Shinjukdo	94	276	46	313	28	199	16	167	17′N, 22′E
Chodo	95	272	45	305	25	193	19	164	14′N, 15′E
Keokumsudo	110	275	53	298	30	189	18	170	30′N, 09′E
Nokdong	116	279	48	297	26	181	19	171	32′N, 08′E

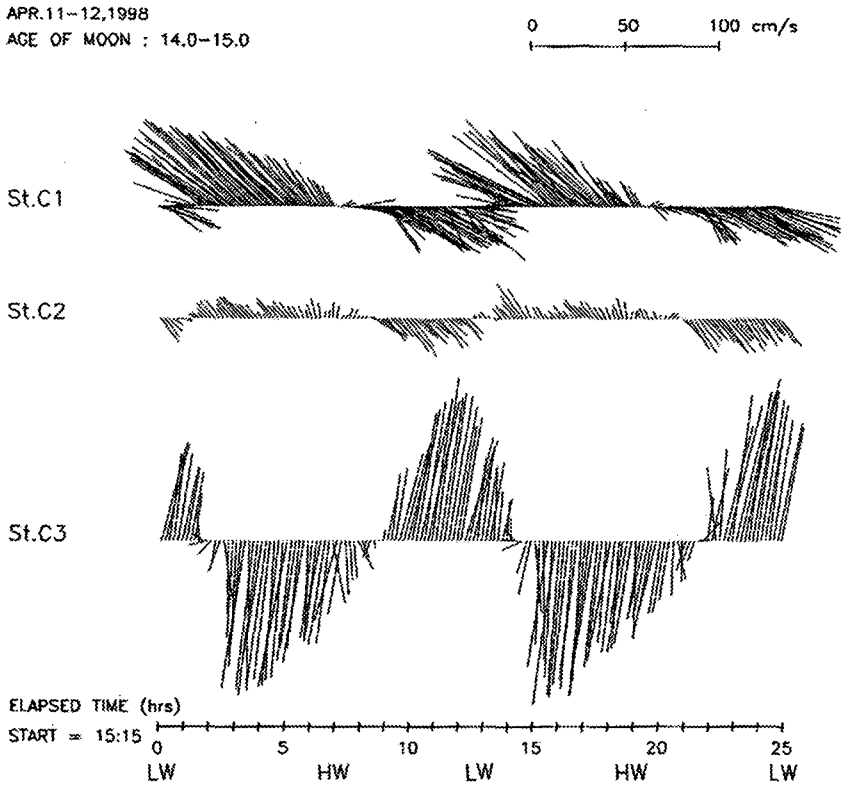

Fig. 2 Stick diagrams of tidal currents at the stations C1~C3.

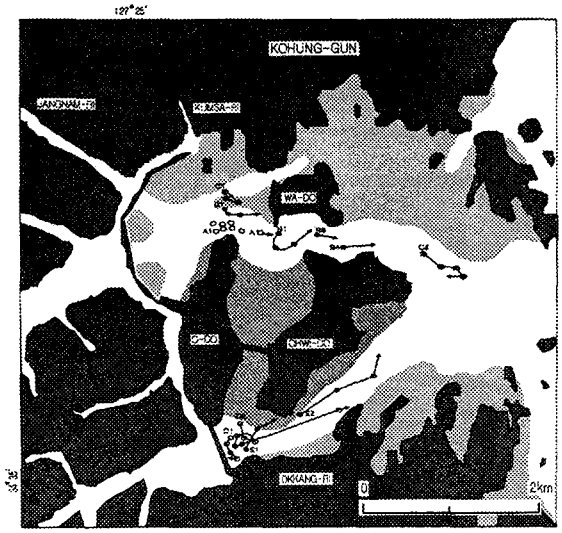

Fig. 3 The tracks of drogues after the freshwater released at the ebb flow.

station C1 and C2 while they flow towards the north at station C3. Although part of the seawater flow into Haechang Bay through the east open boundary at the flood tide, which proceeds up to a tidal embankment, the remainder goes out through the Narodo Channel in the south open boundary. However, the ebb flow is totally opposite to the flood flow.

Fig. 3 typically represents tracks of drogues along with the freshwater released at the opening time(13:40~16:09) of the sluice gates (where the total figure of drogues and drift bottles released was 25). According to the results, the drogues all drifted towards the west and moved out of the bay, but they are not too far from the Wado or Chwido islands because of the comparatively slow currents. Some drift bottles were found around the northwest sluice gates of the bay, due to a weak southwest wind, during that day. As they slightly escaped from the gates due to the different wind speed and direction, it does explain that the flow inside of the bay is active, despite the stagnant flow near the coast with a comparatively shallow water depth.

3.2 Sedimentary Phases

Fig. 4 represents the distribution of sediments at the surface layer for each station. According to the results, the contents of sand turned out to be less than 10 %, except for the areas between the Chwido and Chomdo islands. The contents of silt were 40~50 % at the area between the Chwido and Okkangri, where sluice gate No.2 is located, and 60~70 % at the area between the Odo and Wado islands, where sluice gates No.1 and No.3 are located. Therefore, at the area between the Chwido island and Okkangri the contents of silt tended to increase towards the outer sea while at the areas between the Odo and Wado islands the contents of silt tended to decrease. The contents of clay were 35.6 % on the average and this was found to be extensive all over the bay. However, the contents of clay had a tendency to increase towards the outer sea at the south while they had a tendency to decrease gradually, after a slight increase, at the north.

The distribution of mean grain size is described in Fig. 5. The mean size of grains is 8~9 Φ at the south and 7~8 Φ at the north of the breakwater of Chwido island. As a result, the mean size of grains had a tendency to increase towards the south channel through the Naenarodo. Therefore, the present sedimentary phases can be classified into three different sedimentary phases, such as clayish silt(CSi), Silty clay(SiC) and sandy clayish silt($SCSi$). For instance, a silty clay area between the Chwido and Okkangri, where sluice gate No. 2 is situated, a sandy clayish silt area in front of the Chomdo island and a clayish silt area near the Wado island, where sluice gates No. 1 and No. 3 are situated.

Fig. 6 indicates the skewness, which is an index of reflection for an energy environment when the sediment has been deposited in the present areas. Generally, it is known as the reflection of erosions or non-deposits, if the skewness is less than -0.1. Alternatively, if it is $-0.1 \sim +0.1$, it implies a reflection for the seawater movement and if more than $+0.1$, it implies a reflection for the deposits (Duane[1964]; Folk *et al.*[1964]; Cronan[1972]). The skewness is $-0.1 \sim +0.1$ at the area between the Chwido island and Okkangri, more than $+0.3$ at the area between the Odo and Wado islands, $-0.1 \sim +0.1$ at the area between the Okkangri and Teokheungri and $+0.3$ at the area between the Chomdo island and Namyolri or Teokheungri, respectively. Therefore, it can possibly be judged that the area between the Chomdo island and Namyolri or Teokheungri reflects the phenomena of the seawater movement and the area between the Odo and Wado islands reflects the phenomena of deposits, respectively.

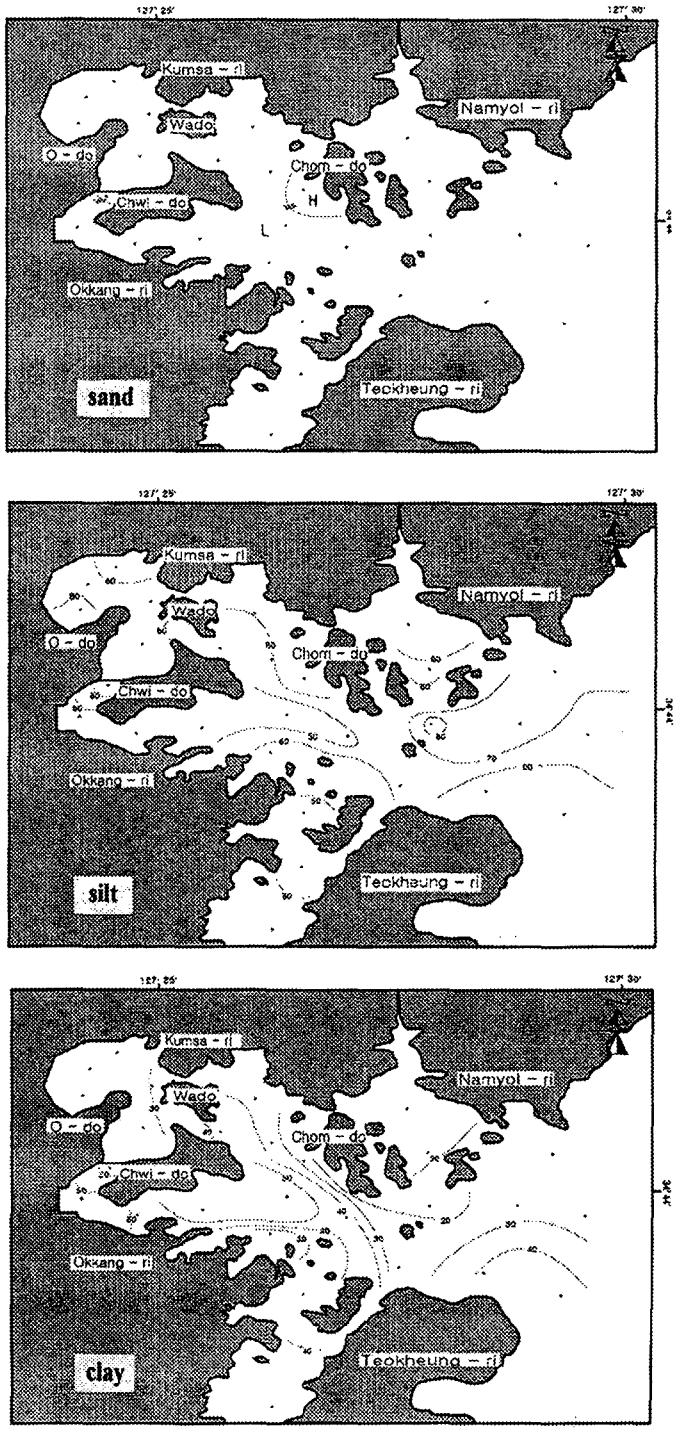

Fig. 4 The distribution of sediments at the surface layer for each station.

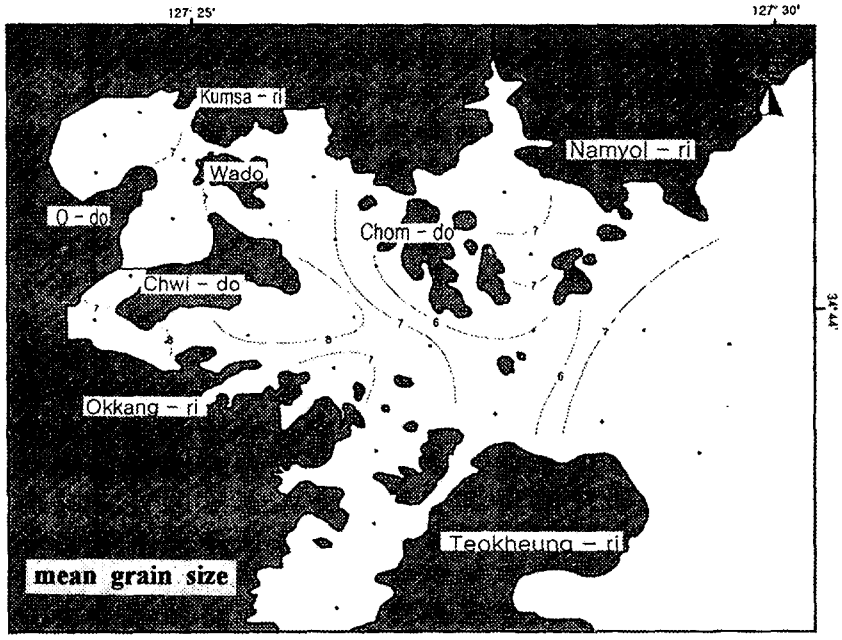

Fig. 5 The distribution of mean grain size.

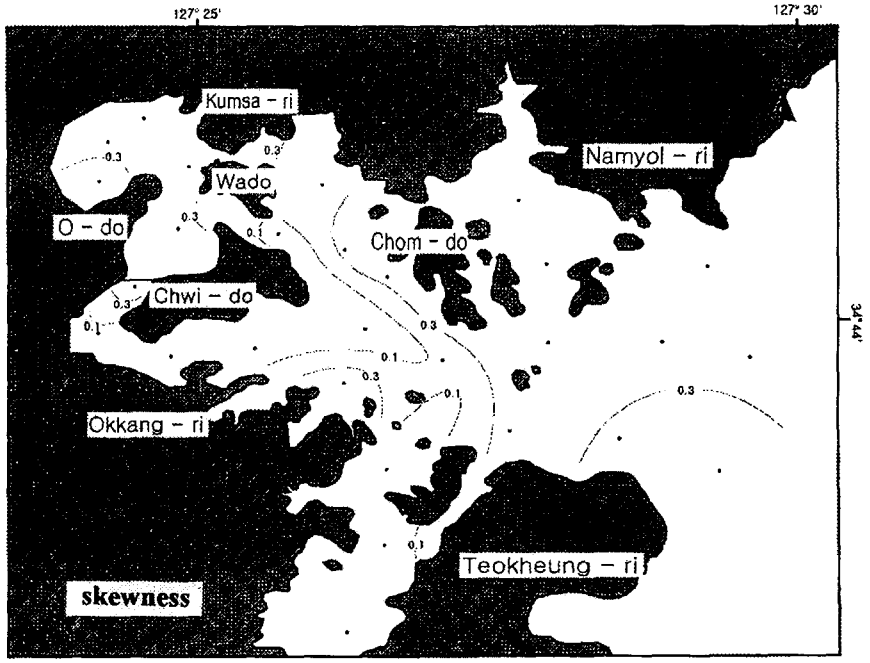

Fig. 6 The distribution of the skewness.

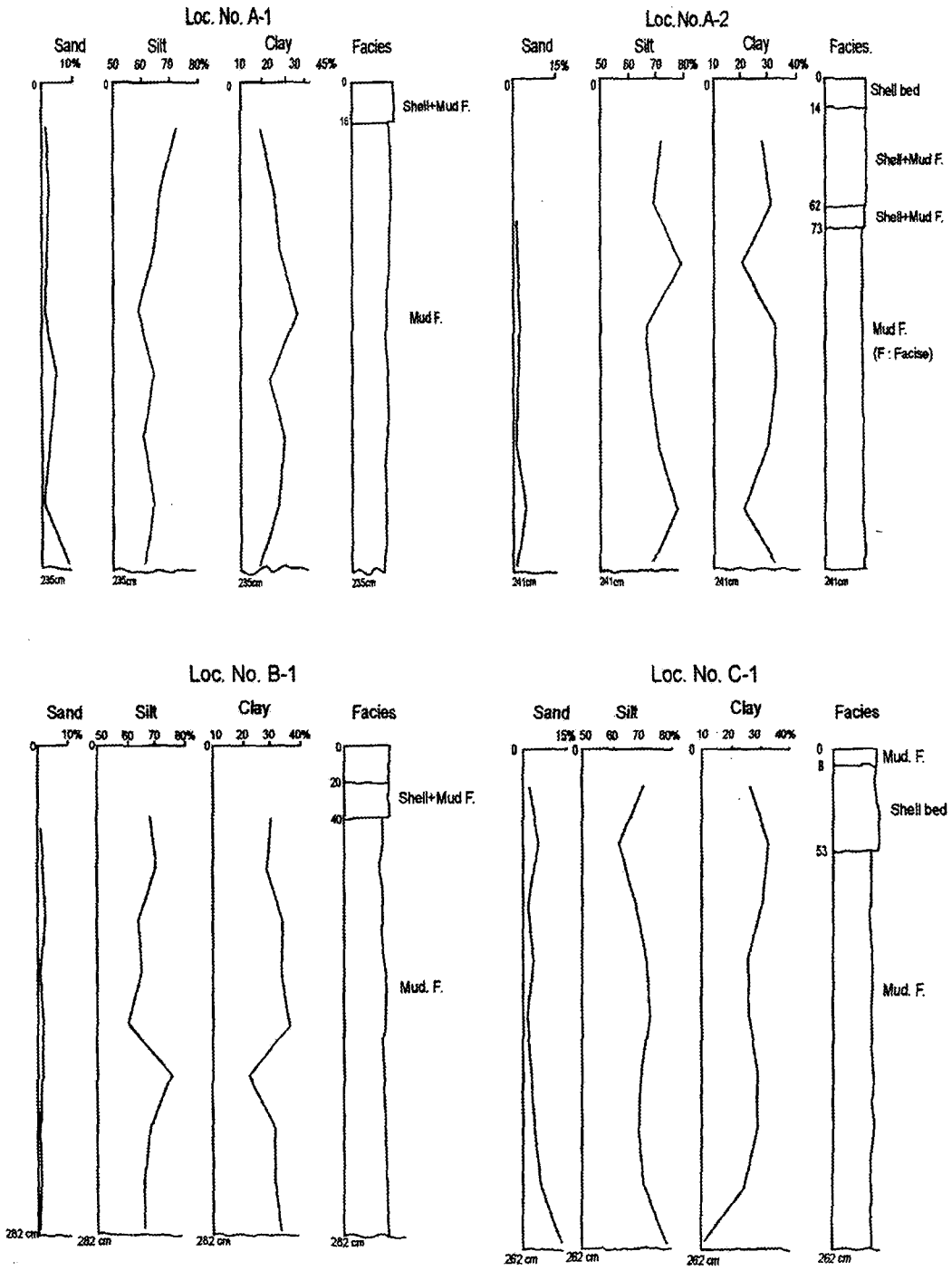

Fig. 7 Profiles of drilling samples showing the variations of sediment composition captured in the vicinity of the embankment.

3.3 Change of Sedimentary Environment induced by Barrage of a Tidal Embankment

In order to investigate the change of sedimentary environment after the reclamation projects and embankment construction, which had been started in 1963, one station(St. 1, as shown in Fig. 2) in front of the embankment has been selected for a drilling with a vibra core, and a sample of 262 cm long has been obtained, as shown in Fig. 7. The analytical results of a drilling sample have shown that the sediment consisted of a muddy layer in reddish yellow with about an 8 cm thickness from the surface. A layer of shellfish mixed with oyster or barnacle towards the middle area and a muddy layer in blackish yellow near the bottom were found, respectively. These distribution patterns explain that muddy layered deposits with the thickness of 53 cm towards the middle from the lower part of sample and a shellfish layer at the upper part would have been formed under different environmental circumstances each other. In other words, the change of sedimentary environments, induced by a physical factor, such as the construction of a tidal embankment would have contributed as a major parameter to the formation of the upper shellfish shell layer.

3.4 Change of Seawater Behaviour induced by Bage of a Tidal Embankment

Fig. 8 is the comparison between field data of tidal current ellipses at stations C1 and C3 as seen in Fig. 1, and computational results, obtained from some iterative computations with a trial and error, using the tidal harmonic constituents seen in Table 2. We assumed that there is no discharge of freshwater from the sluice gates. The computational results favorably reproduced field data in the directions and magnitudes of semi-diurnal tidal currents. So these states of boundary conditions have been fixed as open boundary conditions of the flow field.

Fig. 9 show comparisons of current velocity variations in the maximum flood and ebb flows of the spring tide before and after the construction of a tidal embankment, respectively. After the barrage of a tidal embankment, the velocities of the currents in the bay decreased more than 10 cm/s as a whole, in particular in the vicinity of the barrage. However, the patterns or velocities of the flow out of the bay seemed to be unchanged.

On the contrary, Fig. 10 are variations of tidal levels before and after the construction of a tidal embankment. The water levels fell at low water while they rose at high water after the barrage was lowered, approximately 1 or 2 cm. In a word, the tidal ranges increased that much.

3.5 Change of Seawater Behaviour induced by Freshwater Discharge

In order to examine how the freshwater discharge influenced on the seawater behaviour in the adjacent seas around the sluice gates after the construction of the barrage, the differences of current velocities between the cases of discharge and no discharge of freshwater are compared in Fig. 11. While there is a freshwater discharge, the velocities of currents varied with a range of about ± 5 cm/s, compared to the case of no discharge of freshwater. In particular, the flood flow was influential rather than the ebb flow.

On the contrary, the comparison of the tidal level differences between the cases of discharge and no discharge of freshwater showed that the tidal levels varied within a range of about ± 2 cm. However, the ranges of variation seemed larger at the low water than those at the high water.

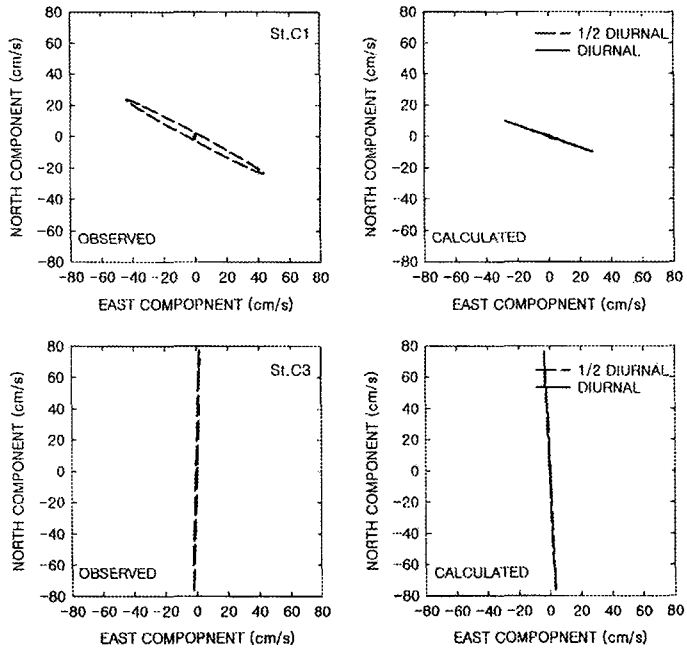

Fig. 8 The comparison of tidal current ellipses between the observed and computed ones.

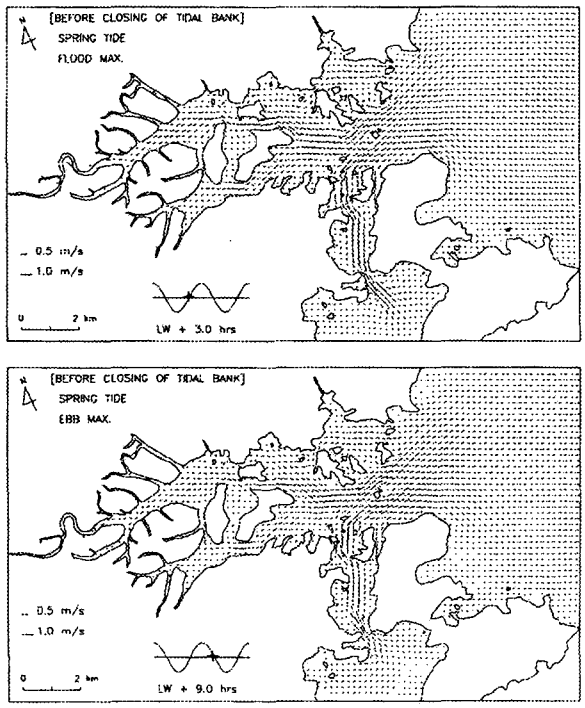

Fig. 9 Comparisons of current velocities between before and after the construction of a tidal embankment.

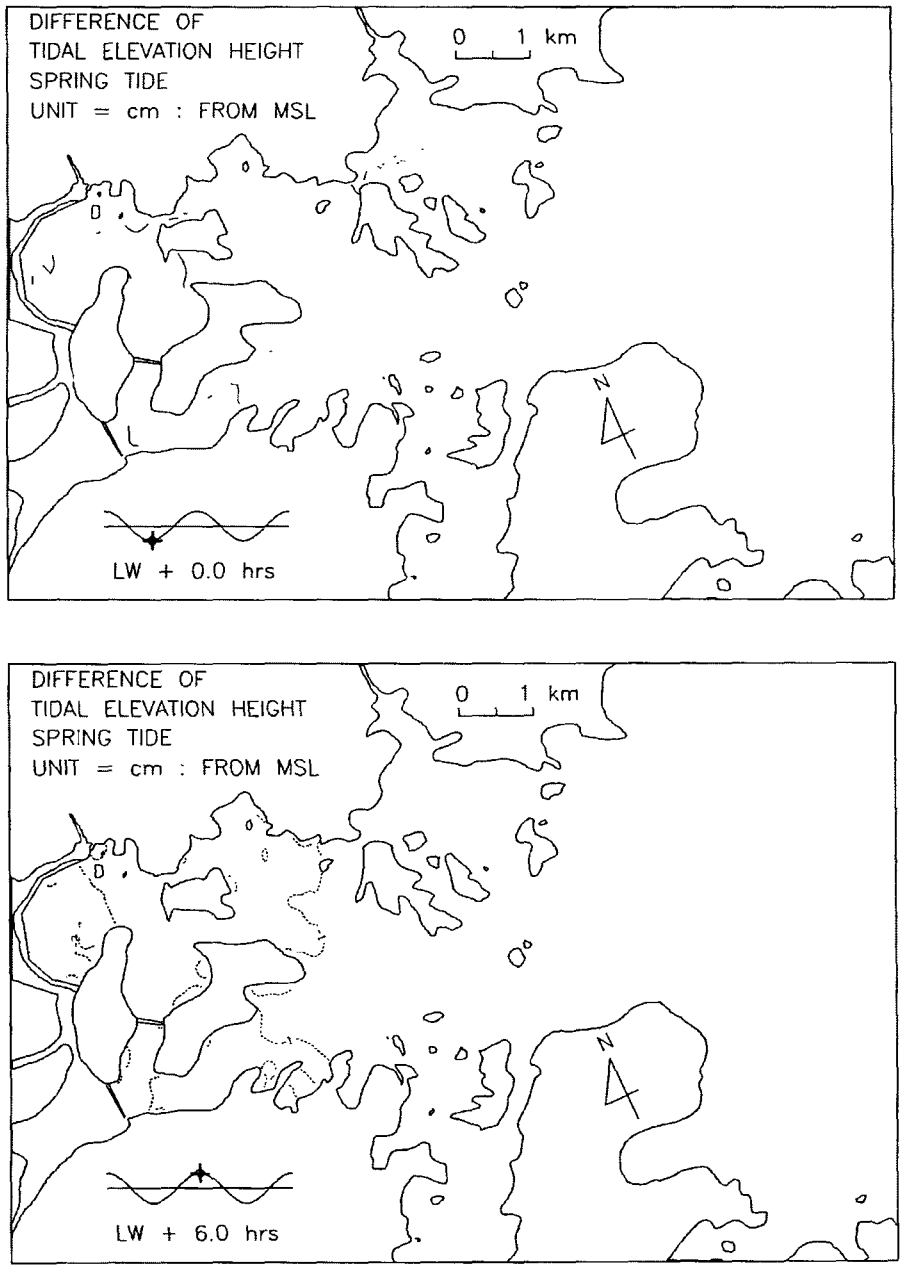

Fig. 10 Comparisons of tidal levels between before and after the construction of a tidal embankment.

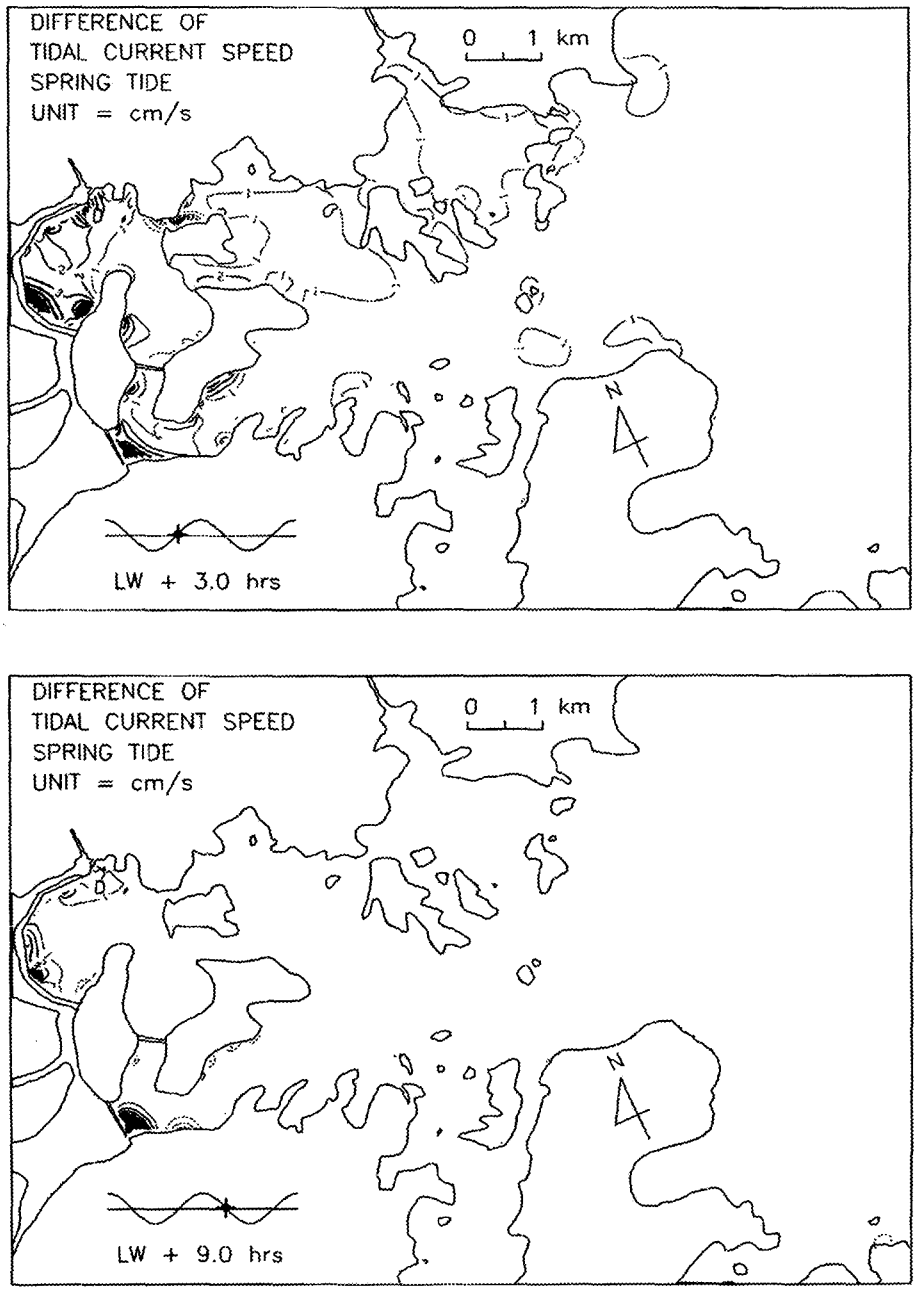

Fig. 11 Differences of current velocities between the cases of discharge and no discharge of freshwater.

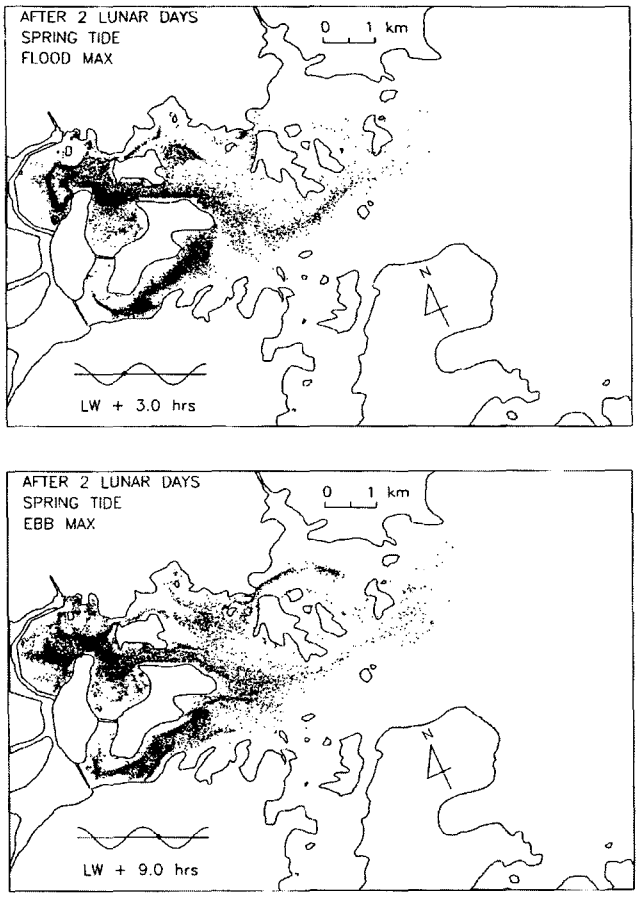

Fig. 12(a) Dispersion of the freshwater released from the sluice gates in terms of a random walk method.

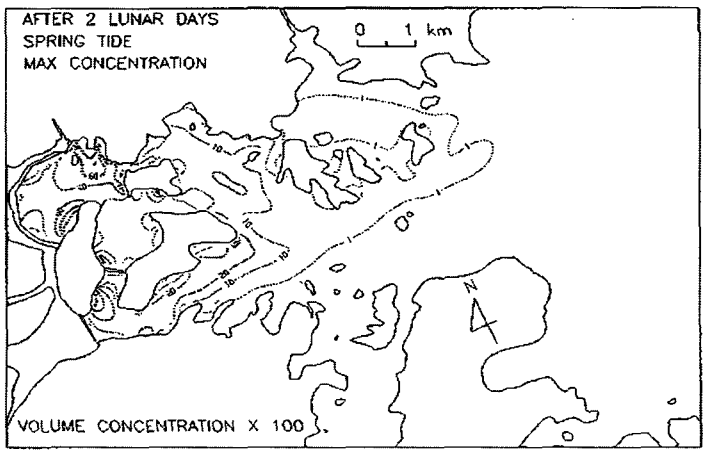

Fig. 12(b) Maximum volume concentration of freshwater two tidal periods after release of freshwater.

3.6 Numerical Experiments of Freshwater Dispersion

As mentioned previously, the computations of freshwater dispersion have been performed to obtain results after two tidal periods from the release of freshwater, assuming the flood and the spring tide. The major aims of this study are to clarify the influences on the surrounding fishing ground while a massive quantity of freshwater is released from the sluice gates.

The freshwater dispersion was calculated using a random walk method. For the accuracy of computation, a three-dimensional baroclinic equation with temperature variations should be solved. However, Haechang Bay is mostly less than 10 m in depth and it has well developed wetlands and irregular variations of water depths. Therefore, for convenience, a two-dimensional numerical model has been adopted in this study. In particular, the study area has insufficient field data for salinity. So instead of solving the equation of salinity directly, we gave the individual freshwater volume per each particle relative to the total volume of released freshwater. Then the non-dimensional volume concentration of the quantity of freshwater relative to the existing seawater was calculated. In this case, the variation of volume concentration should be taken into account due to evaporation or other unknown factors, however, the variation of the quantity of freshwater has been ignored. Because the quantity of evaporation is small and the mechanism of evaporation is also complicated. The numerical model used here is the RNDLEE(Lee *et al.*[1995]) and will be described below.

For a particle of passive contaminant in the flow field, $X(t+\Delta t)$, which is a new position of particle at the time $t+\Delta t$, can be expressed in terms of a drift velocity vector U and a dispersive velocity component u' as follows:

$$X(t+\Delta t) = X(t) + U\Delta t + u'\Delta t \tag{5}$$

The third term on the right side describes the movement of particle due to dispersion and it can be expressed in the probability processes.

$$u'\Delta t = R\sigma \tag{6.1}$$

$$\sigma = \sqrt{2a_L \mid u'(X(t), t) \mid \Delta t} \tag{6.2}$$

where, R is the normal distribution and has 0 as the mean value and 1 the standard deviation. The equations of (6.1) and (6.2) are coincident with a basic solution of diffusion equation without advective terms.

On the contrary, in the probability processes like equations of (6.1) and (6.2), $C(x, y, t)$, which is a probability distribution in the time and the space for individual particle cluster, satisfies the following Fokke-Plank equations.

$$\frac{\partial C}{\partial t} + \frac{\partial (UC)}{\partial x} + \frac{\partial (VC)}{\partial y} = \frac{\partial^2 (D_{xx} C)}{\partial x^2} + \frac{\partial^2 (D_{xy} C)}{\partial x \partial y} + \frac{\partial^2 (D_{yy} C)}{\partial y^2} \tag{7}$$

$$U = u + \frac{\partial D_{xx}}{\partial x} + \frac{\partial D_{xy}}{\partial y} + \frac{D_{xx}}{h}\frac{\partial h}{\partial x} + \frac{D_{xy}}{h}\frac{\partial h}{\partial y} \tag{7.1}$$

$$V = v + \frac{\partial D_{yy}}{\partial y} + \frac{\partial D_{xy}}{\partial x} + \frac{D_{yy}}{h}\frac{\partial h}{\partial y} + \frac{D_{xy}}{h}\frac{\partial h}{\partial x} \tag{7.2}$$

$$D_{xx} = D_L \cos^2\theta + D_T \sin^2\theta \tag{7.3}$$

$$D_{yy} = D_L \sin^2\theta + D_T \cos^2\theta \tag{7.4}$$

$$D_{xy} = (D_L - D_T)\sin\theta\cos\theta \tag{7.5}$$

where, C is a concentration of solute, h is a water depth, $\theta = \arctan(v/u)$, D_L and D_T are the longitudinal and transversal dispersion coefficients of the flow, respectively and described as below.

$$D_L = \alpha_L \mid u'(x(t), t) \mid \tag{9}$$

where, α_L is a mixing length.

The dispersion considers an apparent diffusion due to a vertical velocity distribution into the turbulent diffusion and the longitudinal dispersion coefficient is given by Elder(1959).

$$D_L = 5.93 h U_* \tag{10}$$

where, U_* is a friction velocity which can be obtained from the following equation (11).

$$U_* = \frac{\sqrt{g}}{C}\sqrt{u^2 + v^2} \tag{11}$$

$$C = -18.0 \log \frac{k}{12h} \tag{12}$$

where, C is the *Chezy* coefficient, k is a height of roughness.

In general, the transversal dispersion coefficient D_T accounts for about a quarter of the longitudinal dispersion coefficient D_L. The velocity component due to dispersion in the equation (5), u' can be obtained from the following equation.

$$u_L' = R_1\sqrt{2D_L/\Delta t} \tag{13.1}$$

$$u_T' = R_2\sqrt{2D_T/\Delta t} \tag{13.2}$$

where, R_1 and R_2 are random numbers and have 0 and 1 as the mean value and standard deviation, respectively and the components of dispersion velocity in the x and y directions are as follows:

$$u' = u_L'\cos\theta - u_T'\sin\theta \tag{14.1}$$

$$v' = u_L'\sin\theta + u_T'\cos\theta \tag{14.2}$$

For the Lagrangian particle tracing model, C_{ij}, which is the concentration at each grid point (i, j), is expressed by the following equation (15).

$$C_{ij}(t) = \frac{M}{N}\frac{n_{ij}(t)}{h_{ij}\Delta x \Delta y} \tag{15}$$

where, M is a total quantity of contaminant, N a total number of released particles, n_{ij} a number of particles remaining in the grid point (i, j), h_{ij} a water depth and $m = M/N$, i.e. a quantity of contaminant per each particle.

Fig. 12(a) and (b) represent computational results when the freshwater is discharged from the three sluice gates simultaneously, assuming that a hundred particles of the freshwater per hour are released at each gate during two tidal periods(i.e. fifty hours). Therefore they show results after 30,900 particles of the freshwater were released in total. Fig. 12(a) represents the dispersion of freshwater particles and the distributions of non-dimensional volume concentration at low and high waters at the spring tide, and Fig. 12(b) represents the maximum volume concentration of freshwater, accompanied by the advection and diffusion along with the flow after release of freshwater particles, respectively.

According to the computational results, the freshwater released from the three sluice gates covered the area from the south of Namyolri beyond the Daeokdaedo at low water while it was imposed to return to the inside of Haechang Bay by the westward tidal currents at high water. This trend would also be recognizable in Fig. 12(b), only if the maximum boundary of the freshwater dispersion during the whole release period were identified in terms of the iso-concentration line of 1.0. Basically a scope of the freshwater dispersion coincided with the results predicted by Ryu[1995].

4. CONCLUSIONS

For Haechang Bay, which is located at the south tip of the Kohung Peninsula of Korea, two-dimensional numerical experiments and some field surveys have been conducted to investigate the variations of the flow and sedimentary environment induced by the construction of a tidal embankment; in particular, concerning the fisheries environmental problems, to clarify the impact of a massive quantity of freshwater released instantly from the sluice gates to the adjacent seas. The major results obtained here are as follows:

(1) After construction of the barrage not only the velocities of currents decreased a little but also tidal levels fell, in particular, in the vicinity of a tidal embankment.

(2) When the freshwater is released through the sluice gates, the overall flow patterns never made a big difference compared to the case of no discharge. However, the variations of current velocities and tidal levels near the gates appeared a little, due to freshwater released at the low water.

(3) The computational results of freshwater dispersion showed that the freshwater goes out of the bay at the low water and it returns to the inside of the bay along with the westward tidal currents. This shows a similar tendency with the tracks of drogues and drift bottles at the surface.

(4) The front areas of a tidal embankment had a variety of sedimentary phases, such as clayish silt, silty clay and sandy clayish silt. A clayish silt is prevalent in the middle of the bay. Furthermore, the skewness, which reflects the behaviour of sediments, was ± 0.1 in front of the embankment while it was more than + 0.3 in the middle of the bay. This showed a remarkable difference. Therefore, it can be a good indicator of the impact of freshwater flow induced by periodic operations of the sluice gates of a tidal embankment because it was equivalent to the boundary of freshwater dispersion in the numerical experiments.

(5) Based on the analytical results of the drilling samples obtained at the front area of a tidal embankment, the lower part of the sediments consisted of very fine silt and clayish grains while the upper part consisted of the layer of shellfish such as oyster and barnacle with a thickness of 40~50 cm. Hence, we can deduce that the lower part of sediments would have been an intertidal zone prior to the barrage while the upper shellfish shell part would have been debris induced by some shellfish farms started in the adjacent seas after the barrage. Therefore, the differences in the sedimentary phases indicate the influence of a tidal embankment.

References

[1] Cronan, D.S., 1972, "Skewness and kurtosis in polymodal sediments from the Irish Sea", *Journal of Sed. Pet.*, Vol.42, 102-106.

[2] Duane, D.B., 1964, "Significance of skewness in recent sediments, Western Pamlico Sound", North Carolina, *Journal of Sed. Pet.*, Vol.34, 864-874.

[3] Elder, J.W., 1959, "The dispersion of

marked fluid in turbulent shear flows", *Journal of Fluid Mechanics*, Vol.5, No.4, 544-560.

[4] Falconer, R.A., 1986, "A two-dimensional mathematical model study of the nitrate levels in an inland natural basin", *Proceedings of ICWQM*, BHRA, Fluid Eng., 325-344.

[5] Falconer, R.A. and Chen, Y., 1991, "An improved presentation of flooding and drying and wind stress effects in a two-dimensional tidal numerical model", *Proceedings of Instn. Civ. Engrs.*, Part 2, 91, 659-678.

[6] Folk, R.L. and Ward, W.C., 1957, "Brazos river bar, A study in the significance of grain size parameters", *Journal of Sed. Pet.*, Vol.27, 3-26.

[7] Lee, J.S. and Kim, H.J., 1995, "Sensitivity analysis to the dispersion using a Random walk model", *Journal of the Korean Society of Civil Engineers*, Vol.15, No.5, 1267-1277.

[8] Leendertse, J.J. and Gritton, E.C., 1971, "A water quality simulation model for well-mixed estuaries and coastal seas: Vol.2, Computation procedures", The Rand Corporation, Santa Monica, Report No. RM-708-NYC, 1-53.

[9] Ryu, M.S., 1995, "Damage assessment of fisheries licence due to the sluice gates of freshwater discharge in Haechang Bay", *Report of National Fisheries University of Pusan*, Pusan, Korea, 1-223(in Korean).